vulcanhammer.net
April 2020

DOI: 10.13140/RG.2.2.18499.14884

Inverse Analysis of Driven Pile Capacity in Sands

Don C. Warrington, PhD., P.E.
University of Tennessee at Chattanooga
Department of Mechanical Engineering

Originally to be presented at the University of Tennessee at Chattanooga Research Dialogues, 9-10 April 2020, canceled due to COVID-19. Published online.

Methods of estimating the capacity of driven piles from dynamic pile top data have been well established for many years. The STADYN program uses a finite element methodology that is different from those currently in use. In this paper this program is applied to a well documented pile scenario of concrete piles driven into predominantly cohesionless soils. The pile top force-time and velocity-time history is applied to the model and the results compared with both dynamic tests using conventional methods and static load test results. The results are mixed; the dynamic results compare well with CAPWAP but other factors suggest that more work needs to be done on the STADYN model.

Keywords: pile dynamics, static load tests, CAPWAP, concrete piles, inverse methods

Introduction

The STADYN program–which analyzes impact-driven pile-soil systems to both static and dynamic loading–was originally documented in Warrington (2016). It has been updated in several ways (Warrington (2019a, 2019b); Warrington and Newman (2018)) including the refinement of its performance in clays, testing and refining the program in sands, considering the effect of soil dilatancy, and other improvements and enhancements. STADYN has the capability to analyze a hammer-pile-soil system in forward mode (given pile and soil data and hammer data in some format) and inverse mode (given pile and pile head force-time data, match velocity-time performance with given data by varying the soil properties.)

The ultimate test of the program, however, is the program's performance, when presented with pile top force-time and velocity-time data and a soil profile, during signal matching with the object of developing a soil profile for the pile and thus enabling static load analysis. Such a test was documented in Warrington and Newman (2018); however, the lack of static load test data and other difficulties associated with that pile scenario indicate that different type of scenarios needed to be pursued. With Warrington (2019a) use of the program with both concrete piles and in predominantly cohesionless soils was introduced; however, for a complete scenario both dynamic pile head data and static load test data needed to be obtained.

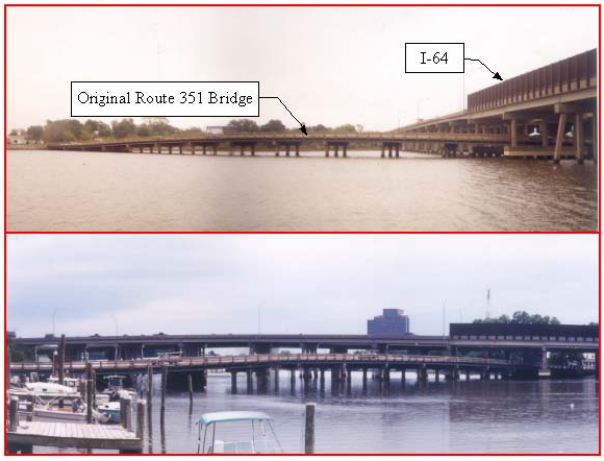

Figure 1. Original Route 351 Bridge (from Pando et al. (2006))

Description of Pile Scenario

Overview

The pile scenario selected for this project was drawn from Pando, Ealy, Filz, Lesko, and Hoppe (2006). Although more than one project and pile type was tested, for this study a test pile for a replacement bridge for VA Route 351 in Hampton, VA was chosen. The bridge (and the I-64 bridge over it) are shown in Figure 1.

Three different pile sizes were tested as part of this program. These are shown in Figure 2. The pile size to be analyzed by STADYN is the 610 mm (20") concrete pile shown

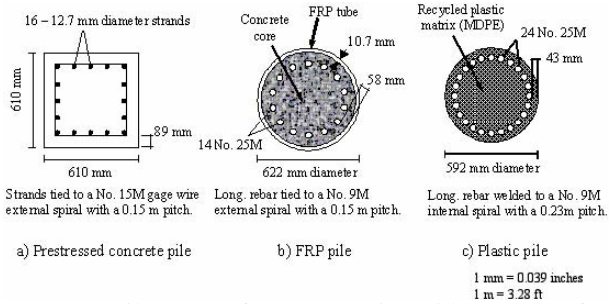

Figure 2. Pile Types for Route 351 Bridge Study (from Pando et al. (2006))

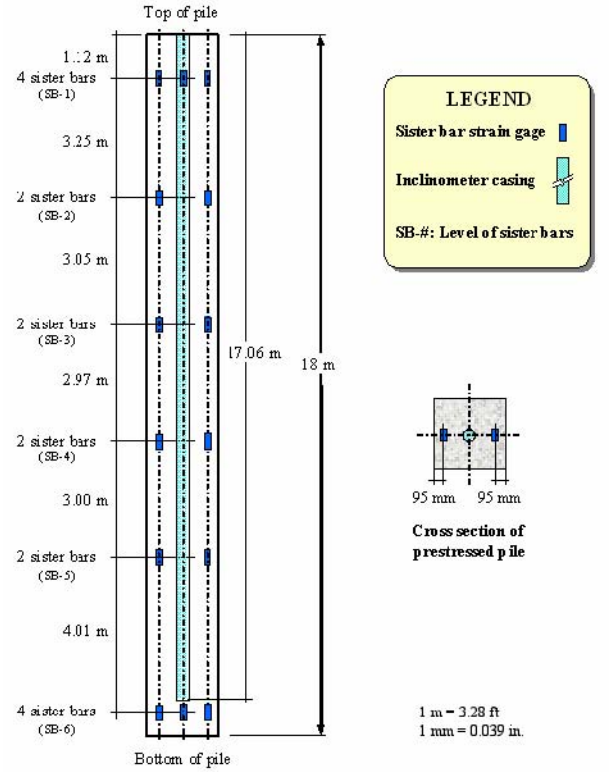

Figure 3. Instrumentation layout for prestressed concrete test pile (from Pando et al. (2006))

at the left. A profile of the pile instrumentation (showing its length) is shown in Figure 3.

The piles were driven into a soil profile as shown in Figure 4. The concrete piles were driven into a soil to a tip elevation/depth of 16.74 m. This was converted to a $\xi - \eta$ profile (Warrington and Newman (2018)) for the forward cases (to be explained below) in Table 1.

During restrike the piles were instrumented and force-time and velocity times impedance-time plots are shown in Figure 5. Also, a static load test was performed on the piles; the pile head load-deflection curves are shown in Figure 6.

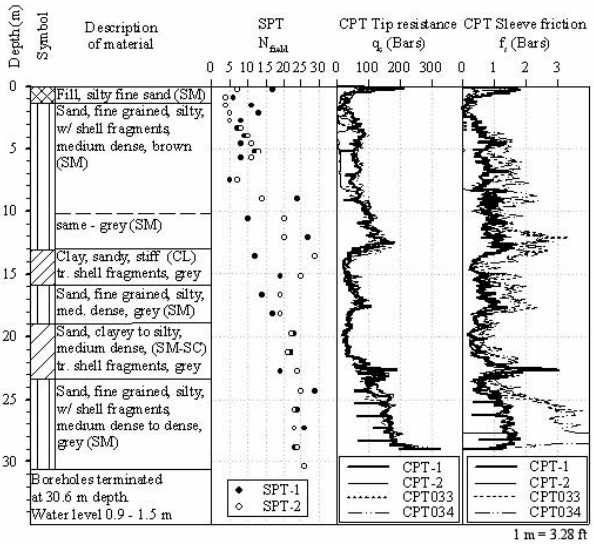

Figure 4. Simplified soil stratigraphy near test pile area (from Pando et al. (2006))

Table 1
Conversion of Data from Figure 4 to $\xi - \eta$ Profile for Cases 1 and 2 (Forward Cases)

Layer	Depth of Layer Bottom, m	ξ	η
1	1.0	-0.8	-0.6
2	1.3	-0.8	-0.6
3	10	-0.8	-0.2
4	13	0.8	0.2
5	16	-0.8	0.2
6	16.8	-0.4	0.2
Toe	33.5	-0.4	0.2

Resolution of Uncertainties in Young's Modulus and Acoustic Speed

The data presentation of the pile and soil system, along with both the static and dynamic response of the pile head, were extensive and made the use of this pile scenario very attractive. There was one issue that complicated the input of the scenario parameters into STADYN, and that was the issue of the concrete pile's actual Young's Modulus and acoustic speed.

To begin, the Young's Modulus was determined from laboratory test and the results are plotted in Figure 7. The value of E from this investigation is around $22,037\,MPa$. Other tests, such as shown in Figure 8, indicate a value of E of around $25,000\,MPa$.

When values of E were applied to STADYN and the velocities were derived based on Figure 5, serious divergence between the velocity values the program returned and those from the dynamic tests. These had not been encountered before with STADYN.

To resolve this problem, consider that, in Figure 5, $^{2L}/_{c}$ =

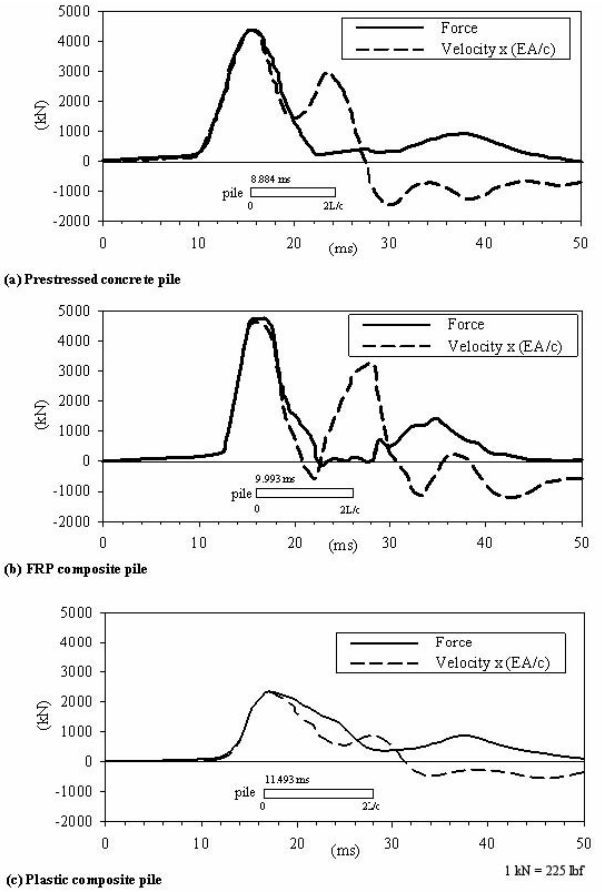

Figure 5. PDA recordings during restrike (from Pando et al. (2006))

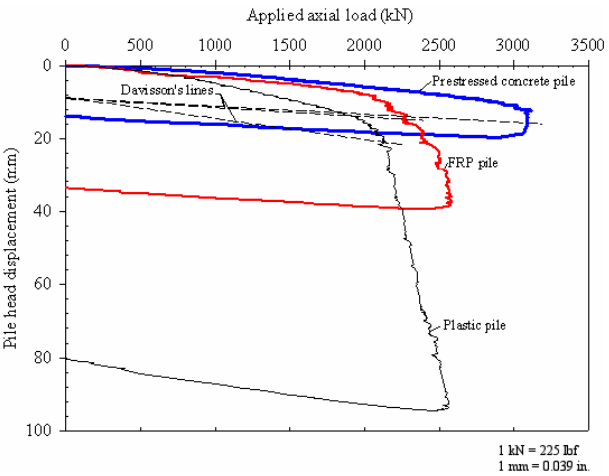

Figure 6. Axial load test results (from Pando et al. (2006))

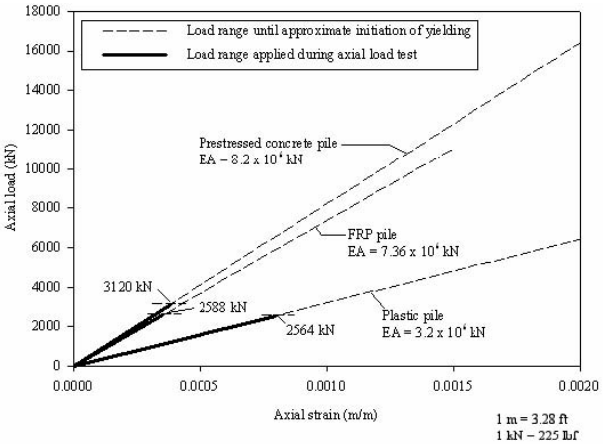

Figure 7. Axial load-axial strain behavior of test piles (from Pando et al. (2006))

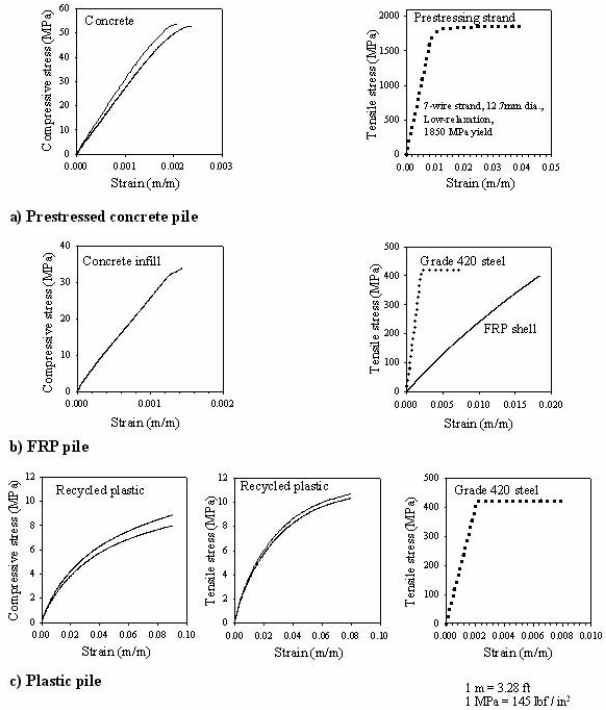

Figure 8. Test pile material properties (from Pando et al. (2006))

8.884 ms. This implies a wave speed of $c = 4,052\,^{m}/_{s}$. Elsewhere in the report other wave speeds are reported. For example, as shown in Table 2, a wave speed of $c = 3,800\,^{m}/_{s}$ was observed. Additionally a pile integrity test (PIT) was conducted, and the results can be seen in Figure 9. The wave speed here is explicitly stated as $4,037\,^{m}/_{s}$, which is close to those from Figure 5.

Using the wave speed value from Figure 5 and a typical concrete density of $\rho = 2,403\,^{kg}/_{m^3}$, a Young's Modulus of $E = 39,454\,MPa$ is obtained. This is higher than the re-

Table 2
Summary of pile-driving measurements for the prestressed and composite piles (from Pando et al. (2006))

Measurement	Pile Type		
	Prestressed	FRP	Plastic
Wave speed	3,800 m/s	3,782 m/s	3,100 m/s
Maximum compression stress measured during driving	11.0 MPa	16.2 MPa	9.9 MPa
Maximum tensile stress measured during driving	5.6 MPa	8.5 MPa	3.3 MPa
Allowable stresses	Comp. < 24.5 MPa Tension < 6.7 MPa	No standards available	No standards available

1 MPa = 145 lbf/inch^2

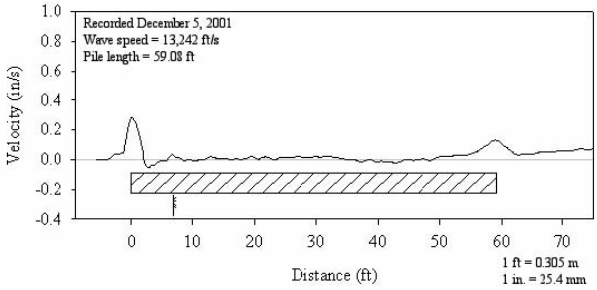

Figure 9. PIT sounding on the prestressed concrete test pile before installation (from Pando et al. (2006))

sults in Figures 7 and 8. These values were used to obtain a pile head impedance of $Z = 3,623\ \frac{kN-s}{m}$, and when these values were applied both to STADYN and the data from Figure 5, the velocity-time histories became much closer. In fact, for the studies described in Warrington (2019a), a Young's Modulus of $E = 32,650\,MPa$ (based on typical values for concrete) was used. The effect of this difference in Young's Modulus will be considered.

Data and Analysis

Test Cases in STADYN

For the data obtained from Pando et al. (2006), five different test cases were analyzed. They were as follows:

1. Forward method, soil layering based on Figure 4, typical concrete Young's Modulus $E = 32,650\,MPa$
2. Forward method, soil layering based on Figure 4, Young's Modulus $E = 39,454\,MPa$ based on project data
3. Inverse method, soil layering based on Figure 4, typical concrete Young's Modulus $E = 32,650\,MPa$
4. Inverse method, soil layering based on Figure 4, Young's Modulus $E = 39,454\,MPa$ based on project data
5. Inverse method, soil layering based on pile discretization, Young's Modulus $E = 39,454\,MPa$ based on project data

The first two divisions in the cases concern the soil layering and the concrete Young's Modulus.

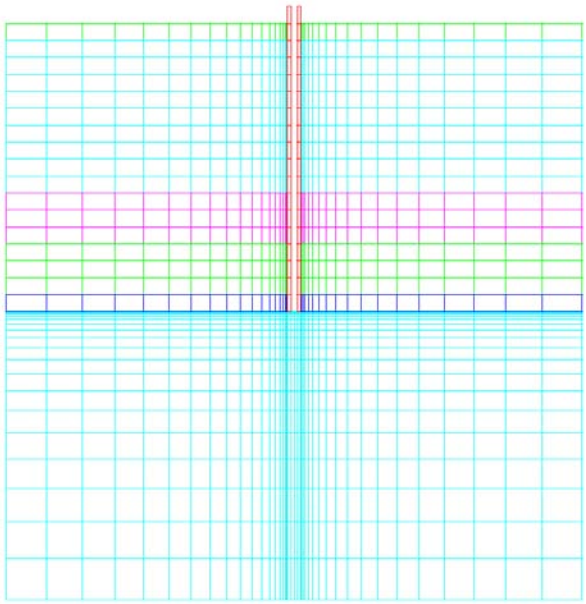

Figure 10. Mirrored Element Map for Layering Based on Figure 4

For forward analysis, the soil profile in Figure 4 was used to input soil properties along the shaft and at the toe of the pile, using the program's $\xi - \eta$ scheme of soil input. For inverse analysis, there were two options available. The first is to use Figure 4 only and to allow the program to ascribe $\xi - \eta$ values to each layer. The second is to use the pile's own discretization to layer the soil. The difference between the two schemes can be seen by comparing the mirrored element models of the two schemes in Figures 10 and 11. It should be noted that, even though the pile is not hollow, STADYN operates in an axisymmetric mode; the pile shown replicates both the perimeter and the cross-sectional area of the original pile. Obviously forward runs will use the layering of Figure 10. Inverse runs were performed with both layering schemes. This was also done in Warrington (2016).

The effects of the change in concrete Young's Modulus can easily be seen by comparing the force-time and velocity-time plots of Figures 12 and 13. Not only do the computed pile head velocities more accurately match the phase of the actual ones, but also for the initial impact the pile head force and the actual pile head velocity-impedance product match each other as they do in Figure 5. One thing that needs to be noted is that, due to the low resolution of Figure 5, some error is encountered in transferring the force-time and velocity-time histories to input for the STADYN program.

Based on this result, Cases 2, 4 and 5, which used the matched Young's Modulus for the pile (and thus its acoustic speed) will be emphasized in subsequent analysis of the data.

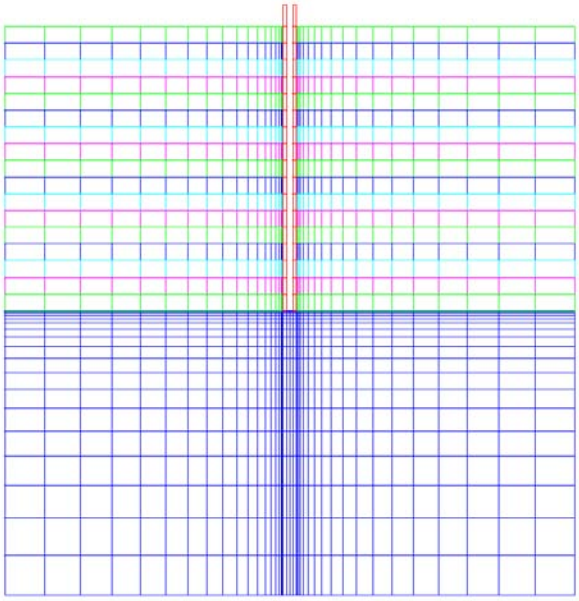

Figure 11. Mirrored Element Map for Layering Based on Pile Discretization ("Full Layering")

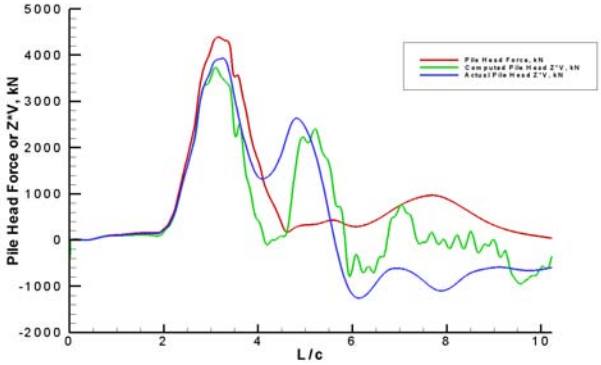

Figure 12. Force-Time and Velocity-Time History, Case 3

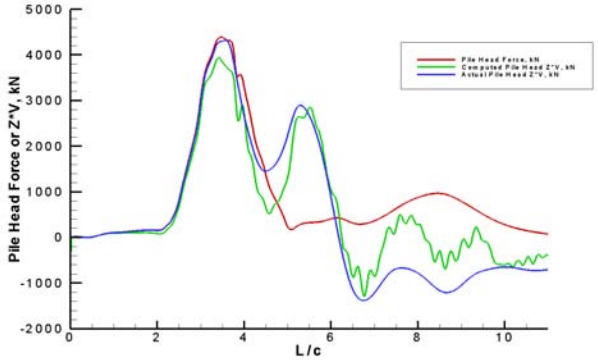

Figure 13. Force-Time and Velocity-Time History, Case 4

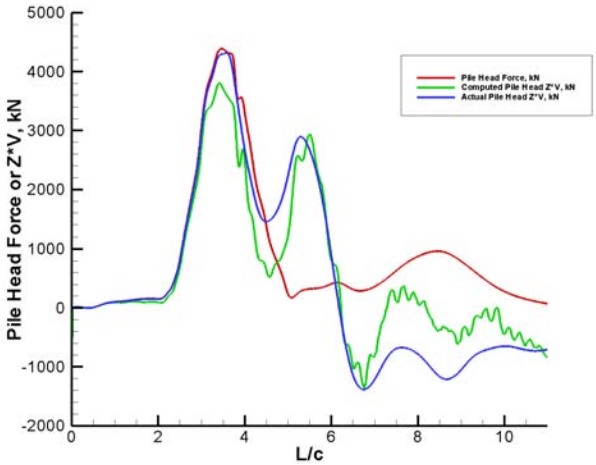

Figure 14. Force-Time and Velocity-Time History, Case 5

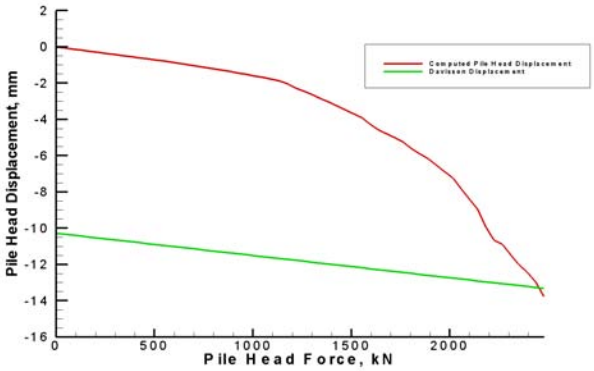

Figure 15. Static Load Test, Case 2

Presentation of Results

The force-time and velocity time results for Cases 2 and 4 were presented in Figures 12 and 13, that for Case 5 in Figure 14. The static load test results for Cases 2, 4 and 5 are presented in Figures 15, 16 and 17.

The optimization tracks represent the values of ξ, η and

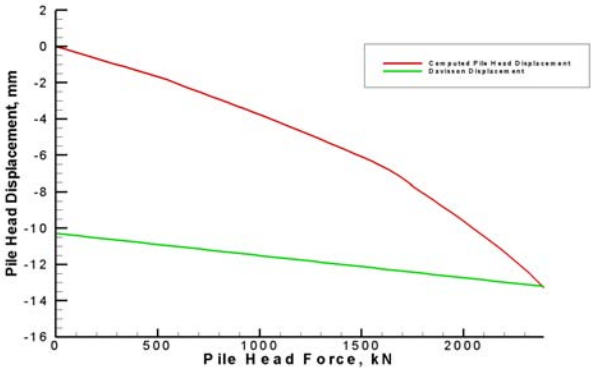

Figure 16. Static Load Test, Case 3

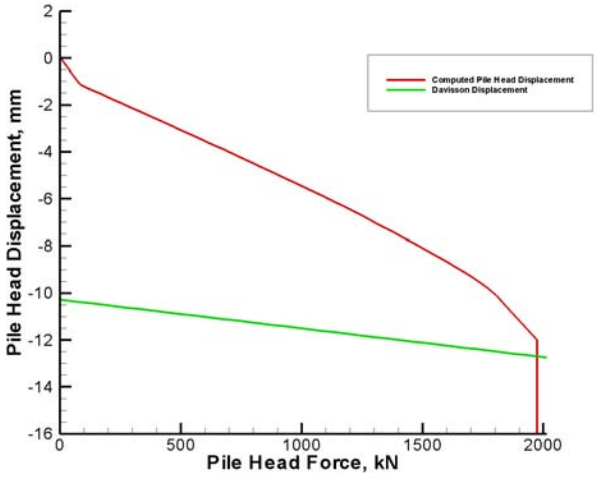

Figure 17. Static Load Test, Case 5

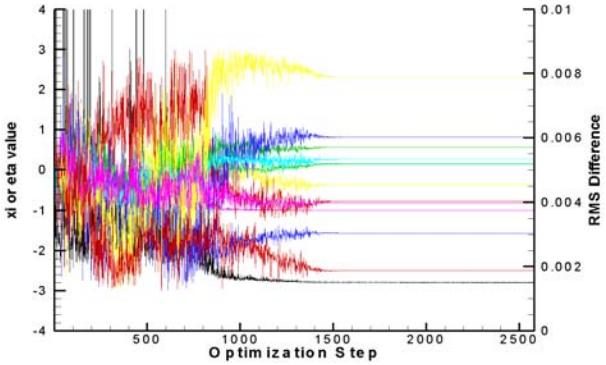

Figure 18. Optimization Track, Case 4

the RMS difference between the computed velocity and the actual velocity as the annealed polytope routine optimized the match between the two velocities. The results for the two inverse cases (Cases 4 and 5) are shown in Figures 18 and 19 respectively. Note that the black line is the RMS difference and has its ordinate on the right side of the graph for both figures. Note also that, in the case of Figure 19, the limitations of the plotting routine did not allow for all of the tracks to be plotted.

A comparison of the results of the layering schemes of the two inverse methods can be found by comparing the $\xi - \eta$ results for each. For Case 4, those results are in Table 3, and for Case 5, Table 4.

A summary of the static and dynamic results for all the cases is shown in Table 5. The actual Davisson static load test result (see Figure 6) was 3095 kN, and from Pando et al. (2006) the restrike CAPWAP ultimate capacity was 1970 kN, with a blow count of 50.4 $^{blows}/_{30\,cm}$, maximum tensile stress of -5.6 kPa, and maximum compressive stress of 11 kPa. If Pando et al. (2006) are correct in attributing the difference of the CAPWAP ultimate capacity and the static load test result

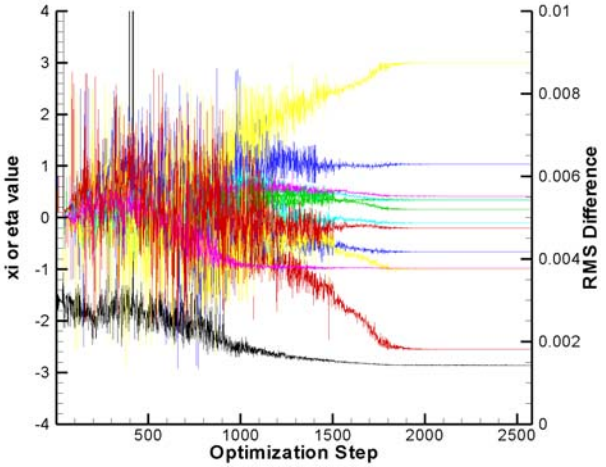

Figure 19. Optimization Track, Case 5

Table 3
Summary of $\xi - \eta$ Results for Case 4

Layer	Depth of Layer Bottom, m	ξ	η
1	1.0	0.141	-1.56
2	1.3	0.141	-1.56
3	10	0.262	-0.370
4	13	-0.993	-0.766
5	16	0.563	0.814
6	16.8	0.155	2.33
Toe	33.5	-0.807	-2.49

Table 4
Summary of $\xi - \eta$ Results for Case 5

Layer	Depth of Layer Bottom, m	ξ	η
1	0.986	0.382	-0.0206
2	1.97	0.0668	-0.665
3	2.96	0.798	0.780
4	3.94	0.262	0.752
5	4.93	0.00121	-0.438
6	5.92	0.226	-1.90
7	6.90	0.719	-0.504
8	7.89	-0.0338	-1.02
9	8.87	0.366	-0.432
10	9.86	-0.189	-0.521
11	10.8	0.354	0.460
12	11.8	-0.985	-0.203
13	12.8	-0.106	-1.01
14	13.8	0.158	-0.664
15	14.8	0.417	-2.55
16	15.8	0.324	3.00
17	16.8	0.359	1.03
Toe	33.5	0.191	0.760

Table 5
Comparison of Basic STADYN Results for All Cases

Case	1	2	3	4	5
Davisson Load, kN	2208	2452	1750	2390	1970
Apparent Set-Up Factor	1.40	1.26	1.77	1.29	1.57
Blow Count, *blows*/30 *cm*	24.6	26.3	35.5	34.8	37.2
Maximum Tensile Stress, MPa	-5.61	-4.37	-3.6	-2.19	-2.85
Maximum Compressive Stress, MPa	12.1	12	12.1	12.1	12
Signal Matching RMS Norm	N/A	N/A	0.00207	0.0015	0.00142

Table 6
Length-Weighted Average Values for $\xi - \eta$

Case	Weighted ξ	Weighted η
2	-0.67	-0.05
4	0.07	-0.26
5	0.18	-0.23

to soil set-up, the apparent set-up factor is 1.58, and this is reported for each of the STADYN results in Table 5. Additionally, in order to make a reasonable comparison of the $\xi - \eta$ parameters for the runs shown in Tables 1, 3 and 4, a layer thickness weighted average was performed. The results of this are shown in Table 6.

Discussion of the Results

1. When the actual acoustic velocity/impedance of the pile is matched with the data, the agreement between the peak force and the peak product of the velocity-impedance product was greatly improved (see Figures 12, 13 and 14.) This was also true with the forward methods, because the impedance of the pile head is independent of the analysis technique.

2. The initial peak values of the pile head velocity were underestimated by STADYN; however, the rebound velocity from STADYN had a better match. Curiously, the maximum compressive stress recorded by STADYN was greater, and the tensile stress less, than what was recorded in the field.

3. Of all the runs, Case 2 (Forward Analysis w/matched acoustic speed) had the best agreement of Davisson capacity with the static load test. This was followed by Case 4 (Inverse analysis w/matched acoustic speed and simplified layering) The lowest Davisson capacity estimated by the dynamic runs is Case 5 (Inverse analysis w/full layering;) however, it is also nearly identical in result to the CAPWAP result from Pando et al. (2006). The wide difference between the CAPWAP result and the static load test was attributed to soil set-up. The ξ values used in the forward analysis were done in anticipation of a more cohesionless stratigraphy (see Table 6.) The results from the inverse analysis, however, indicate that the signal matching values of ξ indicate a more cohesive stratigraphy than originally anticipated, at least for the purposes of pile driving analysis.

4. The η values returned in Table 6 indicate that the stratigraphy was looser/softer than was originally anticipated, and this was reflected in the results, especially with Case 5.

5. The weighted averages of Table 6 do not consider the toe properties that were determined during the inverse analysis. The results from Case 4 (Table 3) indicate a near absence of toe resistance, while Case 5 results (Table 4) indicates meaningful toe resistance.

6. The static load test (Figure 6) indicates plunging failure of the pile. The only STADYN run to replicate this, albeit at a lower load, is Case 5 (Figure 17.) The other cases show a more gradual failure mode for the pile.

7. The use of full layer optimization has been avoided until now because increasing the number of variables to be optimized increases the burden on the optimization method, which may affect the results. (The ambiguous result in Warrington (2016) did not shed light on this problem; the results with full layering were widely variant.) Examination of Figures 18 and 19, along with Table 5 shows that a) the full layering optimization takes longer than the reduced, b) both of the optimizations were nevertheless complete with the maximum step cut-off of the program, and c) the signal matching RMS values likewise improved with full layer optimization.

Conclusions

1. It is important, both with STADYN and other programs, to properly match the acoustic speed of the pile material with that observed in the field. This is especially important with concrete and wood piles, where the value of acoustic speed will vary from one project (or even pile) to the next. The actual value of this was obscured in Pando et al. (2006), and it underscores another important point: the need to examine the data carefully in the process of using results of previous research. Many monographs in pile dynamics do not present enough data to use the results in a meaningful way. While Pando et al. (2006) had sufficient data to do this, the method of presentation obscured some important parameters.

2. If compared directly with the static load tests, the forward analysis was the most satisfying. Saying this assumes that the stratigraphy was cohesionless enough to lower set-up. The $\xi - \eta$ system assumes that, at $\xi = 0$, the soils pass from a cohesionless to a cohesive state (or vice versa) and, in the context of the Unified System, have fines which are 50% of the total weight of the soil. This may not be an appropriate break point for purposes of pile driving analysis and assignment of values based on soil type (this may also apply to forward analyses with programs such as GRLWEAP.) Any effort to use inverse results of programs such as STADYN to establish soil types with depth need to be aware of this and other anomalies such as rate differences in soil response.

3. The full-layering scheme produced the best match with GRLWEAP results, although that may not be as meaningful as it looks (see Svinkin (2019).) In reality, how meaning-

ful either result is depends upon the set-up of the soil. At this point STADYN does not have the facility to estimate elevated pore water pressures due to driving, which would improve the results in situations like this. In principle full layering (which is in effect what CAPWAP uses) is superior, but needs further investigation and more case studies to determine whether the additional variables for optimization do not detract from the accuracy of the method.

References

Pando, M. A., Ealy, C. D., Filz, G. M., Lesko, J., & Hoppe, E. (2006). *A laboratory and field study of composite piles for bridge substructures* (No. FHWA-HRT-04-43). McLean, VA: Federal Highway Administration.

Svinkin, M. (2019). Sensible determination of pile capacity by dynamic methods. *Geotechnical Research*, *6*(1), 52-67.

Warrington, D. C. (2016). *Improved methods for forward and inverse solution of the wave equation for piles* (Unpublished doctoral dissertation). University of Tennessee at Chattanooga, Chattanooga, TN.

Warrington, D. C. (2019a, July). *Application of the stadyn program to analyze piles driven into sand* (Tech. Rep.). doi: 10.13140/RG.2.2.22311.09125/1

Warrington, D. C. (2019b, April). Effective hyperbolic strain-softened shear modulus for driven piles in clay. *University of Tennessee at Chattanooga*, *2019 Research Dialogues*.

Warrington, D. C., & Newman, J. C. (2018, March). Inverse method for pile dynamics using a polytope method. *Presented at the International Foundations Congress and Equipment Expo*.